Revista Mexicana de Astronomía y Astrofísica, **35**, 157–171 (1999)

A MODEL FOR TIDAL INTERACTIONS IN IOTA ORIONIS

E. Moreno and G. Koenigsberger

Instituto de Astronomía
Universidad Nacional Autónoma de México

Received 1999 May 24; accepted 1999 August 19

RESUMEN

Se presenta un modelo bidimensional, que incluye la rotación estelar, para el análisis de la interacción en sistemas binarios debido a las fuerzas de marea, con el cual se pueden evaluar las deformaciones de la superficie estelar a lo largo del ciclo orbital. Adicionalmente a los parámetros estelares y orbitales, los parámetros que determinan la magnitud de las deformaciones son la profundidad de la capa externa modelada y la viscosidad cinemática. Notamos que para valores muy pequeños de la viscosidad, aparece un efecto que se puede asociar con turbulencia de las capas superficiales de la estrella. Se aplica el modelo al sistema muy excéntrico ι *Orionis*, encontrando que el radio de la estrella O9 III primaria tiene que ser menor que 15 $R_\odot$, dado que en las observaciones (Gies et al. 1996) no se detectan las amplitudes de oscilación esperadas para radios mayores.

ABSTRACT

We present a two-dimensional tidal interaction model in which stellar rotation is included, allowing the evaluation of the deformations of the stellar surface throughout the orbital cycle. The parameters which determine the magnitude of the deformations, in addition to the stellar and orbital parameters, are the depth of the surface layer which is modeled and the kinematical viscosity. We note that for very small values of the kinematical viscosity, an effect that can be associated with turbulence of the surface layers appears. The model is applied to the highly eccentric binary system ι *Orionis*. We find that the radius of the primary O9 III star must be smaller than 15 $R_\odot$ in order to account for the absence in observations of the expected oscillation amplitudes (Gies et al. 1996).

Key words: **BINARIES: CLOSE — STARS: INDIVIDUAL: ι ORIONIS — STARS: OSCILLATIONS — STARS: ROTATION**

1. INTRODUCTION

The binary system *iota Orionis* (HD 37043 = HD 1899) is an early-type (O9 III + B1 III) system in a highly eccentric orbit ($e = 0.764$) with a relatively short orbital period (29.13 days). Given its semi-major axis $a = 154\ R_\odot$, its orbital separation at periastron is just ~ 2 times the radius of the primary O9 III star. This system has thus been used for studying a variety of effects which arise due to the interaction of two stars in a close binary system, such as wind-wind collisions (Stevens 1988; Pittard 1998), the focusing of the wind by the companion (Stevens 1988; Gies et al. 1996), and tidally induced stellar oscillations (Gies et al. 1996). *Iota Ori* was recently chosen for studying the problem of the varying conditions of the wind-wind interactions throughout the orbit by the XMEGA group (Corcoran et al. 1999), using the ASCA X-ray observatory. The results of these X-ray observations and the optical observations obtained contemporaneously can be found in Pittard et al. (2000) and Marchenko et al. (2000). Numerical simulations of the wind-wind collision in *iota Orionis* presented by Pittard (1998) illustrate the complicated and variable nature of this predicted wind interaction.

Stickland et al. (1987) studied the system in order to determine whether the mass loss rates are enhanced at periastron with respect to other orbital phases. This increase in mass-loss rate is expected because the presence

of the companion's gravitational force significantly lowers the potential well that the material on the stellar surface is required to exceed in order to escape. However, Stickland et al. (1987) did not find a clear trend in this direction. Stevens (1988) then calculated the expected mass loss variability from the primary star, and concluded that increased mass loss by close to a factor of 2 along the line joining the two stars should indeed occur close to the periastron passage, but that the global enhancement is small (less than 2 percent) and thus would escape detection. In addition, the duration of the enhanced mass-loss is very short lived, predicted to occur within ± 0.05 in phase (= 1.45 days) of periastron. Gies et al. (1996) find weak, residual Hα emission which could be associated with this "focused wind", although conclusive evidence supporting this interpretation is yet to be presented.

A more puzzling discrepancy between the theoretical predictions and the observations is the absence of observable non-radial pulsations effects in the primary star due to the large and variable tidal forces as periastron passage is reached (Gies et al. 1996). In a close binary system, the gravitational field of each of the stars acts as an outer perturbing force on its companion, and through the resulting tidal interaction the stellar surfaces are deformed with respect to their unperturbed shape. This deformation, in general, varies with time, and the detailed response depends on the orbital and stellar parameters, the stellar rotation, and the stellar structure (Press & Teukolsky 1977; Zahn 1977; Savonije, Papaloizou, & Alberts 1995; Kumar, Ao, & Quataert 1995; Goldreich & Nicholson 1989). The tidal interactions have been shown to be a mechanism by which a binary system can reach an equilibrium state by the exchange of orbital and rotational angular momentum and energy, through the torques exerted by the tides (Zahn 1977, 1989 and references therein; Hut 1980, 1981). A system is defined to be in an equilibrium state when the orbit is circular, the stellar rotation period equals the orbital period (i.e., corotation), and the equators of both stars lie in the orbital plane.

Clearly, ι *Orionis* is not in an equilibrium state, and strong tidal effects are expected to occur centered on the periastron passage. Gies et al. (1996) present observations obtained to study these tidally induced oscillations in the O9 III primary. They apply the model for tidally induced oscillations presented by Kumar et al. (1995), and find that the expected tidal oscillations in the primary star should have an amplitude of approximately 0.65 km s^{-1}. However, the expected line profile variations in the spectra were not detected. Because of the importance of the theory of tidal oscillations for several areas of research, and because of the success of this theory in predicting the general evolution of binary systems (Giuricin, Mardirossian, & Mezzetti, 1984a,b,c; Goldreich & Nicholson 1989; Verbunt & Phinney 1995), it is important to understand this apparent discrepancy between the theory and the observations.

In this paper we present a simple two-dimensional model, in which the oscillations of individual surface elements are calculated in order to evaluate the stellar surface deformations at all times during the orbital cycle. The model provides an insight into the role that the different physical forces play in distorting the stellar surface, and the dependence of this distortion on the values of the stellar and orbital parameters, and on the viscosity of the gas.

The expectation is that this simple model may in the future be used for studying the role that tidally induced oscillations may play in modifying the wind structure of stars in close binary systems, with respect to the wind structure of single stars. In particular, Koenigsberger & Moreno (1997) and Koenigsberger et al. (1999) have suggested that the strong variations in the wind structure of the Wolf-Rayet binary system HD 5980 in the Small Magellanic Cloud leading up to its recent LBV-type outburst may have been driven by the tidal forces in this eccentric system.

2. DESCRIPTION OF THE MODEL

The two stars in the binary system that is modelled have masses m_1 and m_2, and radii R_1 and R_2. The orbit has a major semi-axis a and eccentricity e. The stellar rotation is characterized by the parameter $\beta = \omega/\Omega$, where ω and Ω are the stellar rotation angular velocity and the orbital angular velocity, respectively. The equators of both stars are assumed to lie in the orbital plane. Each of the stars is analyzed separately by solving the equation of motion for 100 surface elements located along the equator in a thin shell. This thin shell lies deep enough within the atmosphere so that the oscillations can be treated as adiabatic, but high enough so that the amount of mass lying above it is negligible. The main body of the star, interior to the shell, is assumed to behave as a rigid body and the tidal deformation is assumed to occur mainly in the external shell. We focus our analysis on the surface elements of the external shell, and our approach is to solve directly the equations of motion of these elements. Clearly, this approximation of the responding region of the star to only one thin shell is a simplified picture of the true phenomenon. In reality, all layers of the star are subjected to the tidal forces, and the interaction between the response of each layer with its underlying and overlying layers will determine the overall behavior of the oscillations. We can only justify our approach at this time on the basis that the

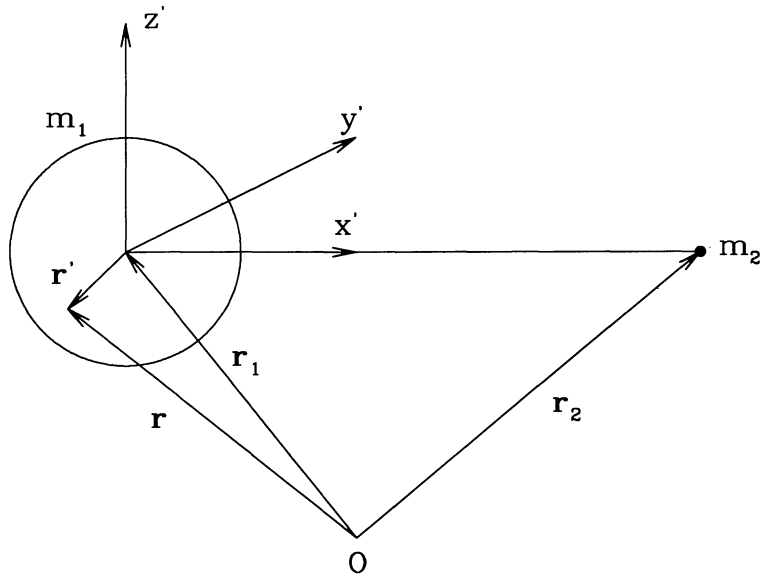

Fig. 1. Non-inertial (primed) Cartesian coordinate system used for the model. This system is centered on the star that is being modelled, m_1, and rotates with the orbital angular velocity of the companion star, located at the point marked with m_2. This companion, m_2, lies in the x', y' plane. The "O" marks the origin of the inertial coordinate system. The orbital motion is in the counter-clockwise direction.

outermost layer of the star is the most susceptible to be affected and that its response can be indicative to first approximation of the expected response of the stellar surface. The general agreement we find in § 3.2 between the velocity amplitudes from our model and the results obtained by Gies et al. (1996) for ι *Ori* using the model of Kumar et al. (1995) is an indication, *a posteriori*, that our simplification may be justified, at least for the calculation of instantaneous surface parameters. For studying the tidal evolution, however, the whole structure of the star will have to be taken into account.

Finally, although we are solving only the motion of the surface equatorial band of the external shell, our results provide some insight into the expected stellar oscillations at latitudes other than the equator.

2.1. *Equations of Motion*

In the two-body problem we take a Cartesian non-inertial reference (primed) coordinate system in which one of the stars, say m_1, is at the origin and the other star is always on the x'-axis. This non-inertial reference system then has an angular rotation velocity with respect to an inertial system equal to the instantaneous orbital angular velocity, $\mathbf{\Omega}$, of m_2 around m_1. In Figure 1 we show the inertial (with origin at the point O) and non-inertial reference systems; an element on the surface of m_1 is located with the vectors $\mathbf{r}$ (inertial) and $\mathbf{r}'$ (non-inertial).

If $\mathbf{a}_{\rm INT}$ is the total inertial acceleration on the element, other than the gravitational due to m_1 and m_2, then the acceleration of the element with respect to the inertial system is (see Fig. 1)

$$\mathbf{a} \equiv \frac{d^2\mathbf{r}}{dt^2} = -\frac{Gm_1\mathbf{r}'}{|\mathbf{r}'|^3} - \frac{Gm_2(\mathbf{r}-\mathbf{r}_2)}{|\mathbf{r}-\mathbf{r}_2|^3} + \mathbf{a}_{\rm INT}, \tag{1}$$

where $\mathbf{r}_1$, $\mathbf{r}_2$ are the positions of m_1 and m_2 with respect to the inertial system. Now, $\mathbf{r} = \mathbf{r}_1 + \mathbf{r}'$ and $\mathbf{a} \equiv \frac{d^2\mathbf{r}}{dt^2} = \frac{d^2\mathbf{r}_1}{dt^2} + \frac{d^2\mathbf{r}'}{dt^2}$. Also

$$\mathbf{a}_1 \equiv \frac{d^2\mathbf{r}_1}{dt^2} = \frac{Gm_2(\mathbf{r}_2-\mathbf{r}_1)}{|\mathbf{r}_2-\mathbf{r}_1|^3}, \tag{2}$$

and the equation connecting the inertial second derivative $\frac{d^2\mathbf{r}'}{dt^2}$ with the corresponding non-inertial $\mathbf{a}' \equiv \frac{d'^2\mathbf{r}'}{dt^2}$ is (Symon 1971)

$$\frac{d^2\mathbf{r}'}{dt^2} = \mathbf{a}' + \mathbf{\Omega} \times (\mathbf{\Omega} \times \mathbf{r}') + 2\mathbf{\Omega} \times \frac{d'\mathbf{r}'}{dt} + \frac{d\mathbf{\Omega}}{dt} \times \mathbf{r}', \tag{3}$$

where $\mathbf{v}' \equiv \frac{d'\mathbf{r}'}{dt}$ is the velocity of the element in the non-inertial system.

With $\frac{d^2\mathbf{r}'}{dt^2} = \mathbf{a} - \mathbf{a}_1$ obtained with equations (1) and (2), equation (3) then gives for $\mathbf{a}'$ the following expression

$$\begin{aligned} \mathbf{a}' &= \mathbf{a}_{\rm INT} - \frac{Gm_1\mathbf{r}'}{|\mathbf{r}'|^3} - Gm_2\left[\frac{\mathbf{r}-\mathbf{r}_2}{|\mathbf{r}-\mathbf{r}_2|^3} + \frac{\mathbf{r}_2-\mathbf{r}_1}{|\mathbf{r}_2-\mathbf{r}_1|^3}\right] - \\ &- \mathbf{\Omega} \times (\mathbf{\Omega} \times \mathbf{r}') - 2\mathbf{\Omega} \times \mathbf{v}' - \frac{d\mathbf{\Omega}}{dt} \times \mathbf{r}'. \end{aligned} \tag{4}$$

This is the equation of motion to solve for each element on the surface of the equatorial shell of m_1.

Taking $\mathbf{r}'$ on the equator of m_1 (plane (x', y')), this plane coinciding with the orbital plane of m_2 around m_1, $\mathbf{\Omega}$ directed along the z'-axis (we take the orbital motion such that $\mathbf{\Omega}$ points in the positive z' direction), and $\mathbf{a}_{\rm INT} = \mathbf{i}'a_{\rm INT_1} + \mathbf{j}'a_{\rm INT_2}$, with $\mathbf{i}', \mathbf{j}'$ unit vectors along the x' and y' axes respectively, equation (4) gives the two scalar equations

$$\begin{aligned} \ddot{x}' &= a_{\rm INT_1} - \frac{Gm_1x'}{(x'^2+y'^2)^{3/2}} - Gm_2\left[\frac{x'-r_{21}}{[(x'-r_{21})^2+y'^2]^{3/2}} + \frac{1}{r_{21}^2}\right] + \\ &+ \Omega(\Omega x' + 2\dot{y}') + \dot{\Omega}y' \ , \end{aligned} \tag{5}$$

$$\begin{aligned} \ddot{y}' &= a_{INT_2} - \frac{Gm_1y'}{(x'^2+y'^2)^{3/2}} - \frac{Gm_2y'}{[(x'-r_{21})^2+y'^2]^{3/2}} + \\ &+ \Omega(\Omega y' - 2\dot{x}') - \dot{\Omega}x' \ , \end{aligned}$$

with $r_{21} = |\mathbf{r}_2 - \mathbf{r}_1|$, Ω , and $\dot{\Omega}$ obtained solving the orbital motion of m_2 around m_1. In this orbital motion we consider a steady orbit, i.e., at this stage we do not take into account the orbital change due to the induced stellar oscillations. Then, if h is the constant orbital angular momentum per unit mass, and u_r the radial orbital speed of m_2, the orbital motion is found solving the equations

$$\begin{aligned} \dot{r}_{21} &= u_r \\ \dot{u}_r &= \frac{h^2}{r_{21}^3} - \frac{G(m_1+m_2)}{r_{21}^2}. \end{aligned} \tag{6}$$

Having at any time r_{21} and u_r, Ω and $\dot{\Omega}$ are obtained with $\Omega = \frac{h}{r_{21}^2}$, $\dot{\Omega} = -\frac{2hu_r}{r_{21}^3}$. Equations (5) for each element and the orbital equations (6) are solved simultaneously.

2.2. *The Inertial Acceleration* $\mathbf{a}_{\rm INT}$

In the non-gravitational inertial acceleration $\mathbf{a}_{\rm INT}$ we include the following forces: (*i*) the internal outward gas pressure force on the surface element, (*ii*) the lateral azimuthal force on the element due to possible different gas pressures exerted by adjacent elements, and (*iii*) the radial and azimuthal viscous forces exerted by adjacent azimuthal elements and by material below the given element, respectively.

(*i*) The Outward Gas Pressure Acceleration

We picture the external equatorial shell as consisting of two regions: an outermost deformable region formed by the surface elements, which can be dragged by the other star, and the inner region which rotates nearly as the main body of the star and expands and contracts in the radial direction. Instead of modelling a detailed radial gas pressure field within this external equatorial shell, we make the simplifying assumption that

the gas pressure below a surface element in the external deformable region is equal to the gas pressure inside the element. This pressure is given by the adiabatic equation $p = p_0(\rho/\rho_0)^\gamma$.

At $t = 0$ the radial velocity of the elements with respect to the center of the star is taken as zero (see § 2.3 for initial conditions). Then if $|\mathbf{a}_{\mathrm{INT}_0}|$ is the initial outward acceleration on the surface element of mass Δm and initial surface area A_0, due to material below it, $p_0 A_0 = |\mathbf{a}_{\mathrm{INT}_0}|\Delta m$. At a later time the corresponding acceleration is $|\mathbf{a}_{\mathrm{INT}_1}| = \frac{pA}{\Delta m} = \left(\frac{A}{A_0}\right)\left(\frac{\rho}{\rho_0}\right)^\gamma |\mathbf{a}_{\mathrm{INT}_0}|$, with A the surface area of the element. Also, with an approximately constant length in the polar direction for each element, the varying length being l in the azimuthal direction, and a depth Δ of the element, we have $\rho/\rho_0 \simeq l_0\Delta_0/l\Delta$ and $A/A_0 \simeq l/l_0$. The ratio Δ_0/Δ is approximated as $\Delta_0/\Delta \simeq (r'_0 - R_0)/(r' - R_0)$, with r'_0, r' the initial and later distances of the surface element to the center of the star, and R_0 the radius of the assumed rigid-body main part of the star. Then the outward acceleration due to gas pressure below the element is approximated as (see equation (15) for $\mathbf{a}_{\mathrm{INT}_0}$)

$$\mathbf{a}_{\mathrm{INT}_1} \simeq \left(\frac{l_0}{l}\right)^{\gamma-1}\left(\frac{r'_0 - R_0}{r' - R_0}\right)^\gamma |\mathbf{a}_{\mathrm{INT}_0}|\mathbf{e}_{r'} \ , \tag{7}$$

with $\mathbf{e}_{r'}$ the radial unit vector.

(*ii*) The Azimuthal Gas Pressure Acceleration

Consider a surface element and its two adjacent elements in the azimuthal direction. Each element has an internal pressure given approximately by an equation of the form $p \simeq p_0\left(\frac{l_0}{l}\right)^\gamma\left(\frac{r'_0 - R_0}{r' - R_0}\right)^\gamma$. The elements are small and thus p_0, l_0, and $r'_0 - R_0$ can be considered as those corresponding to the central element: $(p_0)_c$, $(l_0)_c$, $(r'_0 - R_0)_c$. If $(\Delta S)_c$ is the azimuthal area presented by the central element, then $(\Delta S)_c/(A_0)_c \simeq (\Delta)_c/(l_0)_c$, and for all the elements we take $\Delta_0/(r'_0 - R_0) \simeq \Delta/(r' - R_0) = \delta\ (< 1) =$ const. Then $p_0(\Delta S)_c/(\Delta m)_c \simeq |\mathbf{a}_{\mathrm{INT}_0}|_c(\Delta S)_c/(A_0)_c \simeq \frac{(r' - R_0)_c}{(l_0)_c}|\mathbf{a}_{\mathrm{INT}_0}|_c\delta$.

Thus the azimuthal gas pressure acceleration is

$$\mathbf{a}_{\mathrm{INT}_2} \simeq (r' - R_0)_c(r'_0 - R_0)_c(l_0)_c^{\gamma-1}\left[\frac{1}{l_1^\gamma(r' - R_0)_1^\gamma} - \frac{1}{l_2^\gamma(r' - R_0)_2^\gamma}\right]|\mathbf{a}_{\mathrm{INT}_0}|_c\delta\mathbf{e}_{\psi'} \ , \tag{8}$$

with $\mathbf{e}_{\psi'}$ the unit vector in the azimuthal direction, and of the two adjacent elements the one denoted by 1 having the smaller azimuth.

(*iii*) The Viscous Accelerations

The radial and azimuthal accelerations due to viscous forces are obtained with the shear contribution to the stress tensor (Symon 1971)

$$\mathbf{P}_\eta = -\eta\left[\nabla'\mathbf{v}' + (\nabla'\mathbf{v}')^t - \frac{2}{3}(\nabla'\cdot\mathbf{v}')\mathbf{1}\right] \ , \tag{9}$$

with $\eta = \nu\rho$ the dynamic viscosity and ν the kinematic viscosity (Landau & Lifshitz 1984); $\mathbf{v}'$ is the velocity in the non-inertial system and ∇' is the corresponding spatial operator.

Considering its two lateral faces in the azimuthal direction, the radial viscous force on the central element is given by $\mathbf{F}_{\eta\mathrm{LAT}} = -\mathbf{P}_{\eta_1}\cdot d\mathbf{S}_1 - \mathbf{P}_{\eta_2}\cdot d\mathbf{S}_2$, $d\mathbf{S}_1$ and $d\mathbf{S}_2$ being the lateral azimuthal surface vectors of the central element; $\mathbf{P}_{\eta_1}$, $\mathbf{P}_{\eta_2}$ are the values of the stress tensor on the lateral faces. Writing equation (9) in cylindrical coordinates (r', ψ'), the main contribution to $\mathbf{F}_{\eta\mathrm{LAT}}$ is

$$\mathbf{F}_{\eta r'} \simeq \eta(\Delta S)_c\left[\left(\frac{1}{r'}\frac{\partial v_{r'}}{\partial\psi'}\right)_2 - \left(\frac{1}{r'}\frac{\partial v_{r'}}{\partial\psi'}\right)_1\right]\mathbf{e}_{r'} \ . \tag{10}$$

With the two adjacent elements in the azimuthal direction, we make the gross approximation

$$\left(\frac{1}{r'}\frac{\partial v_{r'}}{\partial \psi'}\right)_1 \simeq \frac{(v_{r'})_c - (v_{r'})_1}{l_c} ,$$
$$\left(\frac{1}{r'}\frac{\partial v_{r'}}{\partial \psi'}\right)_2 \simeq \frac{(v_{r'})_2 - (v_{r'})_c}{l_c} . \quad (11)$$

The radial viscous acceleration is $\mathbf{a}_{\mathrm{INT}_3} = \mathbf{F}_{\eta r'}/\Delta m$. With $\Delta m = \rho l_c (\Delta S)_c$ and $\eta(\Delta S)_c = \nu\rho(\Delta S)_c$ we have

$$\mathbf{a}_{\mathrm{INT}_3} \simeq \frac{\nu}{l_c^2}\left[(v_{r'})_2 + (v_{r'})_1 - 2(v_{r'})_c\right]\mathbf{e}_{r'} . \quad (12)$$

Similarly, the viscous force on the lower face of the element is $\mathbf{F}_{\eta\mathrm{LOW}} = -\mathbf{P}_{\eta\mathrm{LOW}} \cdot \mathbf{A}$, with $\mathbf{A} = -A\mathbf{e}_{r'}$. The main contribution to $\mathbf{F}_{\eta\mathrm{LOW}}$ is

$$\mathbf{F}_{\eta\psi'} \simeq -\eta A\left(\frac{\partial v_{\psi'}}{\partial r'} - \frac{v_{\psi'}}{r'}\right)_{\mathrm{LOW}} \mathbf{e}_{\psi'} = -\eta A\left(r'\frac{\partial \omega'}{\partial r'}\right)_{\mathrm{LOW}} \mathbf{e}_{\psi'} , \quad (13)$$

with $\omega' = v_{\psi'}/r'$ the angular velocity in the non-inertial reference frame. Taking the characteristic distance for the change of ω' at the lower face of the same order as the (small) depth of the element, we have $\left(r'\frac{\partial\omega'}{\partial r'}\right)_{\mathrm{LOW}} \simeq r'(\omega' - \omega'_{\mathrm{INT}})/\Delta$, with ω', ω'_{INT} the angular velocities of the element and of the inner, rigid region, of the star, respectively. With respect to an inertial frame the angular velocity of the inner region of the star is written as $\omega_{\mathrm{INT}} = \beta_0\Omega_0$ (see § 2.3), with β_0 a constant and Ω_0 the initial orbital angular velocity; then $\omega'_{\mathrm{INT}} = \beta_0\Omega_0 - \Omega$. Then with $\Delta m = \rho A\Delta$ and $\Delta = (r' - R_0)\delta$ the azimuthal viscous acceleration $\mathbf{a}_{\mathrm{INT}_4} = \mathbf{F}_{\eta\psi'}/\Delta m$ is

$$\mathbf{a}_{\mathrm{INT}_4} \simeq \frac{-\nu r'(\omega' + \Omega - \beta_0\Omega_0)}{(r' - R_0)^2\delta^2}\mathbf{e}_{\psi'} . \quad (14)$$

Finally, with equations (7), (8), (12), and (14), the non-gravitational inertial acceleration is $\mathbf{a}_{\mathrm{INT}} = \sum_{i=1}^{4}\mathbf{a}_{\mathrm{INT}_i}$.

2.3. *Numerical Method and Initial Conditions*

We have divided the equatorial shell of the star into 100 surface elements. The motion of these elements is obtained solving eqs. (5) and (6) simultaneously for all the elements. A seventh-order Runge-Kutta algorithm (Fehlberg 1968) has been applied. The initial shape of the stellar surface is spherical with an equal separation l_0 between the mid-points of the elements along the shell; at later times the local separation gives the azimuthal length l of the element. To generate arbitrary initial conditions of motion of the elements, we have taken $\mathbf{a}_{\mathrm{INT}_0}$ as if $\mathbf{a}'$, $\mathbf{v}'$ and $d\boldsymbol{\Omega}/dt$ in equation (4) were zero at t = 0; then $\mathbf{a}_{\mathrm{INT}_0}$ is

$$\mathbf{a}_{\mathrm{INT}_0} = \left\{\frac{Gm_1\mathbf{r}'}{|\mathbf{r}'|^3} + Gm_2\left[\frac{\mathbf{r} - \mathbf{r}_2}{|\mathbf{r} - \mathbf{r}_2|^3} + \frac{\mathbf{r}_2 - \mathbf{r}_1}{|\mathbf{r}_2 - \mathbf{r}_1|^3}\right] + \right.$$
$$\left. + \boldsymbol{\Omega} \times (\boldsymbol{\Omega} \times \mathbf{r}')\right\}_{t=0} . \quad (15)$$

The initial radius of the surface is taken as the major semi-axis of the approximate prolate shape of m_1 in the instantaneous hypothetic equilibrium represented by equation (15). The initial velocity of the elements is purely azimuthal, and depends on the parameter β_0, defined as the ratio between the initial stellar angular velocity (i.e., the angular velocity of the surface elements), ω_0, (with respect to an inertial reference system) and the initial orbital angular velocity, Ω_0. In eccentric orbits, this ratio changes as the star goes from apastron to periastron. Thus, at an arbitrary time during the orbital cycle, we define $\beta = \omega/\Omega$. The system is corotating when β=1.

The radius R_0 is taken, in general, $R_0 = 0.99\ R_*$, with R_* the mean equilibrium radius of the star, and the constant δ (defined previous to equation 8) is given values of the order $\delta \sim 0.1$ to 0.5.

TABLE 1

PARAMETERS FOR ι *ORIONIS*

Parameter	Value	Reference
Spectrum	O9 III + B1	Stickland et al. (1987)
m_1 ($M_\odot$)	38.9	Stickland et al. (1987)
m_2 ($M_\odot$)	18.9	Stickland et al. (1987)
R_1 ($R_\odot$)	15.8 ± 3.2	Stickland et al. (1987)
R_2 ($R_\odot$)	9.6 ± 1.9	Stickland et al. (1987)
a ($R_\odot$)	154	Stickland et al. (1987)
e	0.764	Stickland et al. (1987)
V_P sin i (km s^{-1})	120	Gies et al. (1996)
V_S sin i (km s^{-1})	80	Gies et al. (1996)
i (°)	47	Stickland et al. (1987)

3. MODEL CALCULATIONS FOR ι *ORIONIS*

The ι *Orionis* parameters required for the model calculations are listed in Table 1. Stickland et al. (1987) provide a range of values for the radii of the stars in the system, based on the uncertainties involved in their determination. We will analyze two models for the O9 III primary star, one with a radius near the upper end of the range ($R_1 = 18.0\ R_\odot$) and one at the lower end ($R_1 = 12.6\ R_\odot$). The values of the rotational velocities of the two stars in the system (Gies et al. 1996), give values of $\beta \sim 0.5$. Thus, the stars are not co-rotating at periastron. At apastron, where the calculation is started, the rotation velocity of the primary star gives values of $\beta_0 = 28$ (for $R_1 = 18.0\ R_\odot$), and $\beta_0 = 36$ (for $R_1 = 12.6\ R_\odot$). With the system parameters and β_0 fixed, the only variables for the calculation are the values of the kinematical viscosity, ν, the depth of the external equatorial shell, $(r'_0 - R_0)/R_1 = H$, and the fraction of this external equatorial shell which is allowed to be "dragged" in the horizontal direction by the gravitational force of the companion, δ. For the present calculations, we have maintained $H = 0.01$ also fixed. The effects for other values of H will be discussed in § 3.4.

In Table 2 we list input parameters and some of the results of typical model runs in which the deformation of the surface of both stars has been analyzed for values of ν between 0.07 and 10 $R_\odot^2$ day^{-1}(1.0 $R_\odot^2$ day^{-1}= 5.6×10^{16} cm^2 s^{-1}) and δ between 0.2 and 0.5.

The degree of deformation is quantified with the parameter R_{max}= max$[R_i]$, the maximum radius achieved by the star in a given direction at any given time. The radii R_i correspond to the 100 individual surface elements, with R_1 belonging to the surface element which faces the companion at the time the calculation is started. The "tidal bulge" coincides with the set of surface elements that include R_{max}. The line which crosses the R_{max} element and the center of the star defines its major axis at any particular time. The angle Θ_{bulge} is used to denote the position of this major axis with respect to the line joining the centers of the two stars. The maximum deformation of the star occurs near periastron, at which time the tidal bulge is pointing in the general direction of the companion.

The first column of Table 2 lists the value of the radius the star would have if it were a single star; column 2 lists the maximum value obtained for R_{max} in the timespan covered by the calculation; columns 3 and 4 contain, respectively, the value of δ and ν that were used; column 5 lists ΔR_{max}, the maximum amplitude of oscillation in units of the star's radius; and columns 6 and 7 contain the values of Θ_{bulge} at periastron and apastron, respectively.

3.1. *Time-Varying Tidal Bulge Amplitude and Orientation*

In this section we will describe in detail the results of the model for the $R_1 = 18.0\ R_\odot$ case of the primary O9 III star in ι *Orionis* for values $\delta = 0.2$ and $\nu = 0.07\ R_\odot^2$ day^{-1}. The models with other combinations of δ and ν display very similar behaviors. In Figure 2*a* we illustrate the time-varying amplitude of the tidal bulge for a timespan of 500 days (16 orbital cycles). When the calculation is started, the system undergoes a transitory

TABLE 2

MODEL RUNS FOR ι *ORIONIS*

R_1 ($R_\odot$)	max(R_{max}) ($R_\odot$)	δ	ν ($R_\odot^2$ day^{-1})	$\Delta R_{max}/R_1$	Θ_{bulge}(peri) (°)	Θ_{bulge}(ap) (°)
Secondary Star						
9.6	9.618	0.5	0.1	1.4×10^{-3}	−10	−38
9.6	9.630	0.5	0.05	2.7×10^{-3}	−12	−30
9.6	9.622	0.2	0.01	1.7×10^{-3}	−16	−33
Primary Star						
18.0	18.09	0.5	1.0	3.9×10^{-3}	0	−35
18.0	18.09	0.5	0.5	3.9×10^{-3}	− 3	−35
18.0	18.11	0.5	0.2	5.0×10^{-3}	−10	−30
18.0	18.10	0.3	0.1	4.2×10^{-3}	−10	−35
18.0	18.09	0.2	0.07	3.9×10^{-3}	− 2	−30
18.0	18.08	0.2	1.0	3.9×10^{-3}	0	var.
18.0	18.077	0.2	10.0	3.7×10^{-3}	0	var.
15.0	15.028	0.2	0.1	1.2×10^{-3}	− 5	+50
12.6	12.611	0.2	0.3	4.7×10^{-4}	− 2	+40

period of adjustment (lasting nearly four orbital cycles), after which the amplitude of the bulge oscillation becomes repetitive, reaching maximum values at periastron passage. The total amplitude of the oscillation associated with the bulge is typically 0.06 $R_\odot$ corresponding to a deformation of $\sim 10^{-3}$ from its equilibrium position. Figure 2*b* illustrates an amplified portion of Figure 2*a*.

The orientation of the bulge at periastron passage is nearly in the direction of the companion (Θ_{bulge}∼-2°), as is illustrated in Figures 3*a* and 3*b*. Just after periastron, however, the tidal bulge starts to "lag" behind the orbital motion, and two days later Θ_{bulge} ∼-20°, after which time it begins to advance systematically. As illustrated in Figure 3*b*, the major axis of the star rotates periodically around the star until the next periastron passage, with a period of 5.8 days. This motion is such that at apastron, the tidal bulge lags by ∼ 30°.

The vertical displacements of the surface elements are associated with velocities in the vertical direction. In analogy with the value of R_{max} shown in Figure 2a, we illustrate in Figure 4*a* the value of the maximum vertical velocity $(v_r)_{max}$ for an interval of time well after the initial transitory period. The maximum velocity (2 km s^{-1}) is attained a few hours before periastron passage, as is illustrated in Figure 4*b*. Also evident in this figure is that the only large velocity amplitudes occur within a time interval of ± 0.5 day around periastron, although small-amplitude oscillations (< 0.2 km s^{-1}) are present throughout the cycle. Also of interest is the azimuth angle at which the maximum velocity occurs, and this is illustrated in Figure 4*c*. At periastron, maximum velocity occurs at the surface element which is located at azimuth angle +10°.

It is important to distinguish between the maximum velocity attained by the elements, $(v_r)_{max}$, and the velocity attained by the R_{max} element. At any given time, the surface element with the largest radius (i.e., R_{max}) and the surface element with the largest outward velocity (i.e., $(v_r)_{max}$) are different surface elements. The R_{max} element undergoes velocity changes as illustrated in Figure 5, where one can see that its maximum velocity occurs prior to periastron, before R_{max} has achieved its largest value. The time of periastron is indicated by the filled-in square, and we have superposed with a thinner tracing the corresponding values of R_{max} (scaled to fit the figure). Evident also on this figure are short-timescale oscillations, with a period of ∼ 0.12 day (∼ 2.9 hours) throughout the orbit.

In Figure 6 we illustrate the shape of the equatorial region of the star at periastron and apastron. The abscissa and ordinate display, respectively, the azimuth angle and the radius of the corresponding surface element. In this figure, the data for two periastron and apastron passages are superposed, showing that the shape of the star repeats consistently from one orbital cycle to the next. The tidal bulge facing the companion is significantly narrower ($\Delta\Theta \sim 50°$ FWHM) than the bulge on the opposite side ($\Delta\Theta \sim 115°$ FWHM).

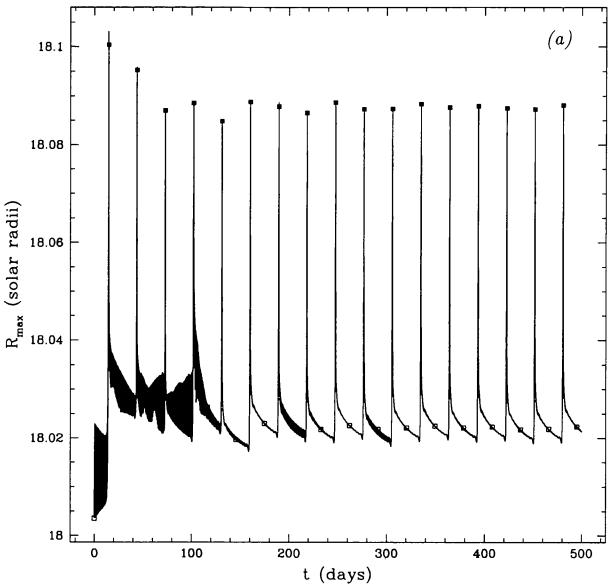

Fig. 2*a*. Amplitude of the maximum radial displacements in the O9 III primary star in *iota Orionis*. The squares indicate the times of periastron (near the maximum) and apastron (near minimum). The large amplitude, high frequency oscillations present throughout the first few orbital cycles are a consequence of the (non-equilibrium) initial conditions at which the calculation was started.

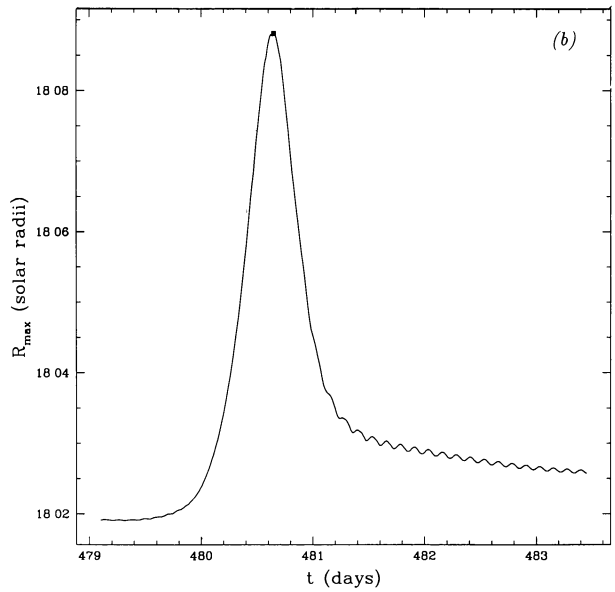

Fig. 2*b*. Amplified portion of Fig. 2*a* illustrating the time of periastron (filled-in square), and the small scale radial oscillations whose amplitude is greatest after periastron.

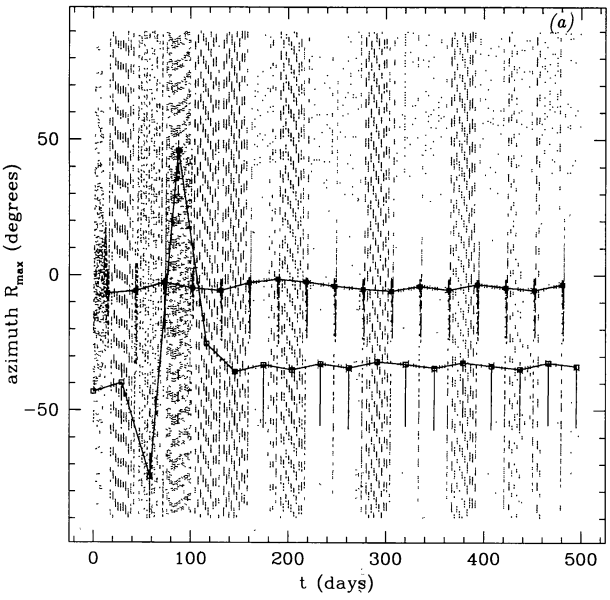

Fig. 3*a*. Variation of the azimuth angle at which R_{max} occurs. The solid lines are drawn in to guide the eye in locating the periastron and apastron passages. At periastron, R_{max} is always at an azimuth angle of $\sim -2°$ (i.e., the tidal bulge "lags behind"). At apastron, it "lags behind" by $\sim 30°$. At other phases it can be pointing in any direction.

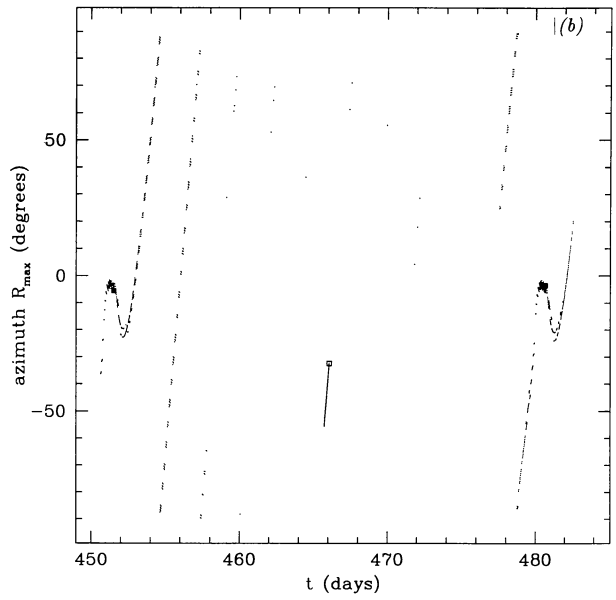

Fig. 3*b*. Amplification of Fig. 3*a* illustrating the periodic nature of the rotation of the major axis of the primary star throughout the orbital cycle, and the rapid reversal around periastron passage (filled-in squares).

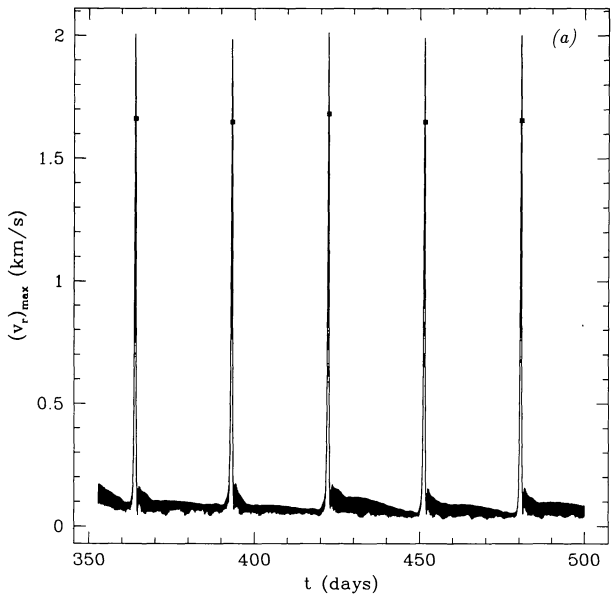

Fig. 4*a*. Maximum velocity in the radial direction of surface elements as a function of time. The time of periastron occurs just after maximum (indicated by the square).

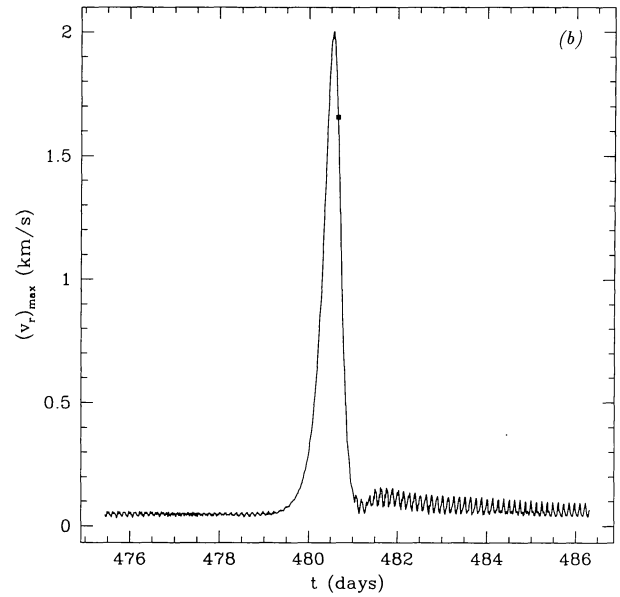

Fig. 4*b*. Amplified portion of Fig. 4*a* illustrating the maximum value of the velocity in the radial direction as a function of time around periastron (indicated by the filled-in square) and the small-scale oscillations.

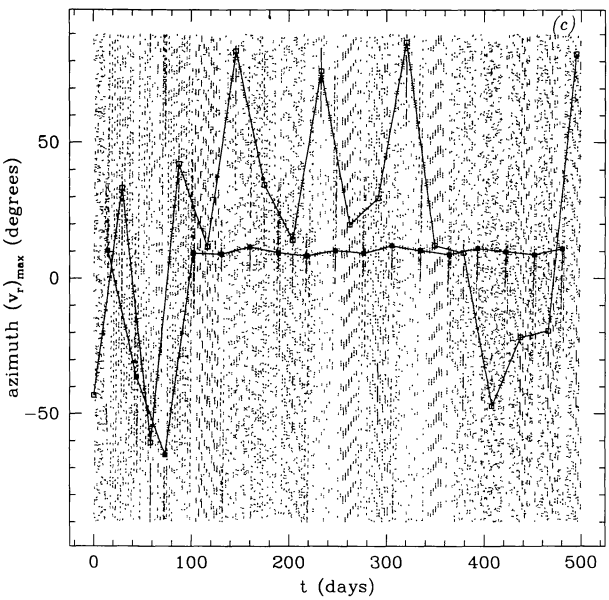

Fig. 4*c*. Azimuth angle of the surface element at which the maximum velocity in the radial direction is found, as a function of time. Periastron and apastron passages are marked by the filled-in and open squares, respectively.

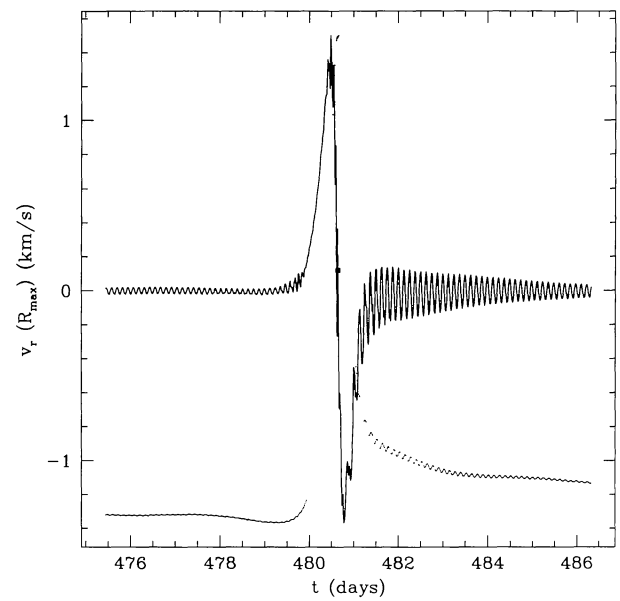

Fig. 5. Velocity in the radial direction of the surface element where R_{max} is attained (dark line). The time of periastron is marked with the filled-in square. The broken line is the (scaled) shape of the R_{max} oscillation (same as in Fig. 2*b*).

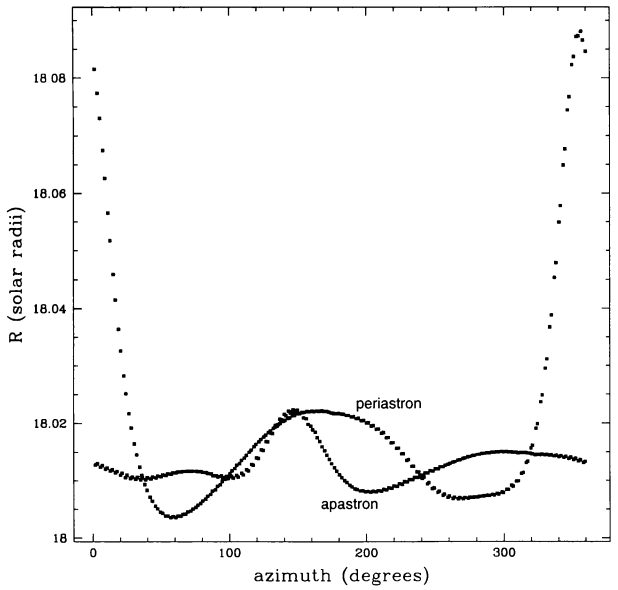

Fig. 6. Radius of each of the 100 surface elements as a function of azimuth angle at periastron and at apastron for the primary O9 III star. Azimuth angle $\Theta = 0$ corresponds to the element which is directly facing the companion. Data for two periastron and apastron passages are overplotted.

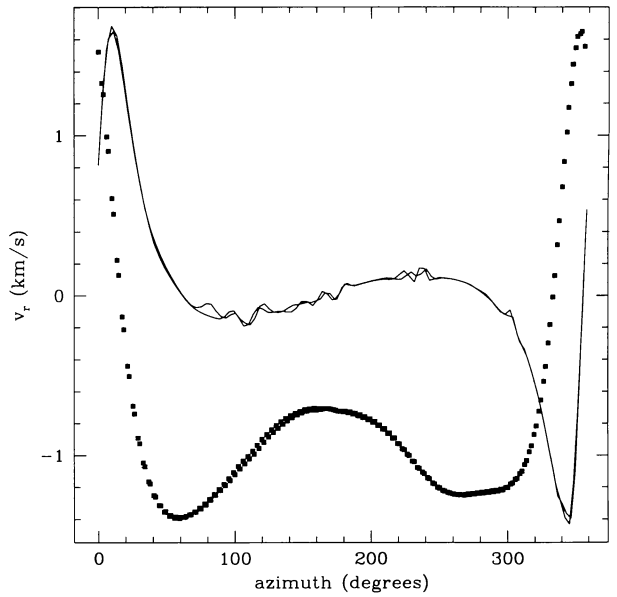

Fig. 7. Velocity in the radial direction (solid lines) of each of the 100 surface elements of the primary star as a function of azimuth angle at periastron. Two different periastron passages are plotted. The filled-in squares are the (scaled) values of the radii of the corresponding surface elements (same as in Fig. 6 for periastron).

Evident also in Figure 6 is the smooth variation in the position of each surface element with respect to its neighboring elements. That is, the edge of each surface element remains in contact with the neighboring elements. This smooth variation along the equator of the star is also present in the radial velocity components of the elements at periastron. This is illustrated in Figure 7 where we plot the velocity in the radial direction for each of the 100 surface elements as a function of azimuth angle (solid lines), together with a plot of the (scaled) radii of these elements (the same as in Fig. 6). Two different periastron passages are plotted, illustrating the repeatability of the behavior of the surface from one cycle to another. The maximum velocity ($+1.6$ km s^{-1}) at periastron occurs at an azimuth angle of $\sim +10°$, while the minimum value (~ -1.4 km s^{-1}) occurs at $-20°$.

The smooth velocity curve at periastron depicted in Figure 7 does not persist very much beyond the time of periastron passage. It is gradually replaced by a "choppy" velocity curve, where different portions of the stellar surface have different velocities, but with very small amplitudes (0.005 km s^{-1}). The "choppy" patterns repeat from cycle to cycle.

The analogous calculation for the secondary star results in a behavior which is qualitatively, very similar to that of the primary star, but with quantitative differences. Due to its smaller radius, the tidal bulge oscillation amplitude is two times smaller than the primary's bulge, and the maximum radial velocity amplitude (~ 0.2 km s^{-1}) is ten times smaller than in the companion. The period for the short-timescale oscillations is 0.07 day (1.6 hours).

3.2. *Dependence on the Stellar Radius*

The amplitudes of oscillation are governed to a large extent by the value of the stellar radius. Smaller radii result in smaller oscillation radial velocity amplitudes. For ι *Ori*, the lower limit of the range of values possible for the primary star's radius is 12.6 $R_\odot$ (Stickland et al. 1987). The value of the radial velocity amplitude obtained from our model computed for this radius is $(v_r)_{max} \sim 0.12$ km s^{-1}. For an intermediate value $R_1 = 15\ R_\odot$, $(v_r)_{max} \sim 0.4$ km s^{-1}. This value is consistent with the value of 0.65 km s^{-1} computed by Gies et al. (1996) using the Kumar et al. (1995) model assuming a (larger) stellar radius of 15.8 $R_\odot$. This leads us to the conclusion that the non-detection by Gies et al. (1996) of the expected 0.65 km s^{-1} amplitudes provides an upper limit to the stellar radius of the primary star in ι *Ori* of 15 $R_\odot$.

3.3. *The Effects of the Viscosity*

From the perspective of the computations carried out in this investigation, the kinematical viscosity is the parameter which plays an important role in keeping the outer layers of the star coupled to the innermore layers, and preventing them from being freely dragged over the more rigid interior as they respond to the gravitational pull of the companion at periastron. It is also through the effects of the viscous forces that oscillations are damped. The values of ν we have used here (0.07 to 10 $R_\odot^2$ day^{-1}) correspond to values of the dynamical viscosity, $\eta \sim 4 \times 10^{11} - 5.6 \times 10^{13}$ gm cm^{-1} s^{-1} for densities typical of giant stars, or to values $\sim 4 \times 10^{13} - 5.6 \times 10^{15}$ gm cm^{-1} s^{-1} for densities typical of main sequence stars (cf. Lang 1986). This range in dynamical viscosities coincides with the viscosity demanded by the short timescales for circularization of the orbits of early-type stars (Alexander 1973; Sutantyo 1974).

For the models we have computed here, we find that there is a lower limit of ν below which our computations must be stopped. When these small values of the viscosity are used, the smooth shape of the star at periastron (such as that illustrated in Fig. 6) breaks down, and the surface elements whose motion is being followed begin to overlap and cross over each other. For the current parameters, and with $\delta = 0.5$, this occurs in the secondary star with $\nu = 0.01\ R_\odot^2$ day^{-1} and in the primary star ($R_1 = 18.0\ R_\odot$ case) with $\nu = 0.1\ R_\odot^2$ day^{-1}. By reducing the value of δ, it is possible to reduce the value of ν without reaching a critical state at which the overlap of surface elements appears in the computation. Thus, by using $\delta = 0.2$ we were able to compute the models with $\nu = 0.07\ R_\odot^2$ day^{-1}. This effect in which the surface elements overlap for small values of the kinematical viscosity is suggestive of turbulence and it is interesting to note that the values of ν we require to maintain the identity of the inividual surface elements is on the order of magnitude of the turbulent viscosity discussed by Press, Wiita, & Smarr (1975). However, given the current limitations of our model (i.e., the thin surface layer located only on the equator of the star and no radiation pressure), it would be premature to speculate further on this topic.

In Figures 6, 8*a* and 8*b*, we illustrate the effect that increasing the value of ν has on the stellar shape of the primary star at periastron and at apastron. At periastron, there is only a slight decrease in the amplitude and azimuth angle of the tidal bulge as larger values of ν are used. The effects of increasing the viscosity are more obvious at apastron, where for the larger values of ν there is nearly no distortion of the stellar surface. In

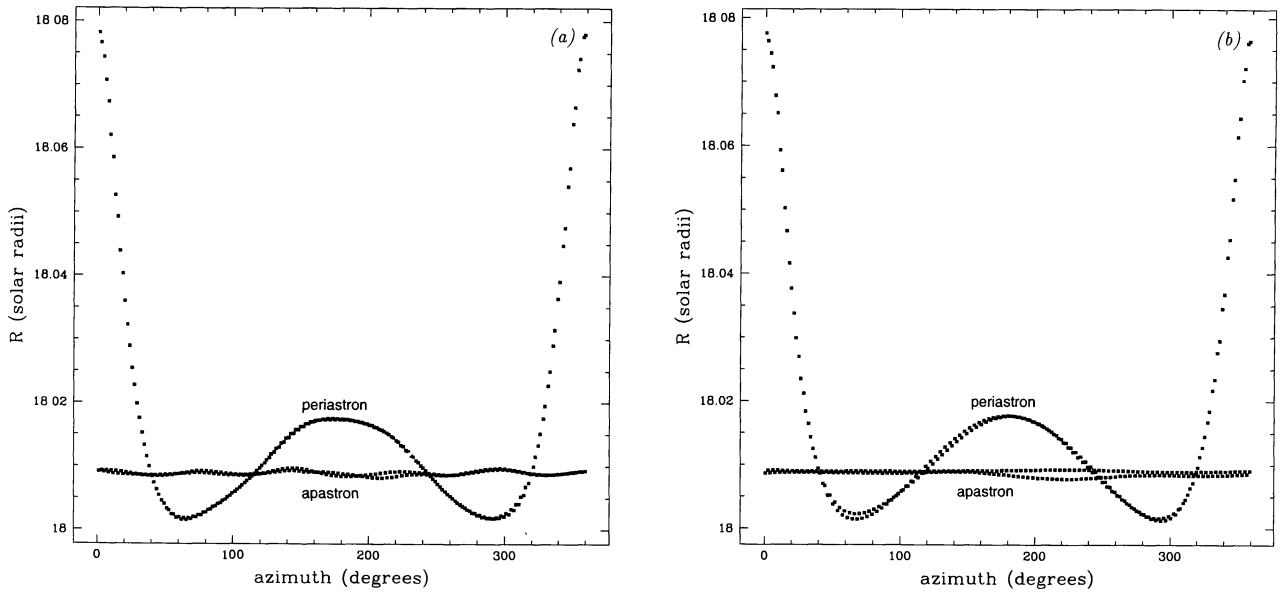

Fig. 8*a*). Radius of each of the 100 surface elements at periastron and apastron (two passages each) for the primary star, for a model computed with $\delta = 0.2$ and with the kinematical viscosity $\nu = 1.0\ R_\odot^2$ day^{-1}. Note the greatly diminished deformation at apastron, compared with Fig. 6, where $\nu = 0.07\ R_\odot^2$ day^{-1}. *b*) Same as Fig. 8*a*, but with $\nu = 10\ R_\odot^2$ day^{-1}.

these figures more than one periastron and apastron passage are plotted. We note that the repeatability of the curves from one orbit to another is not as precise for the $\nu = 10\ R_\odot^2$ day^{-1} as it is for the others. This is the result of the much longer computing times required for the large ν, and that the computation for the $\nu = 10\ R_\odot^2$ day^{-1} case was stopped before the initial transitory phase had fully terminated (although the stage where the velocity amplitudes at periastron are reliable had already been reached).

3.4. *Dependence on the Depth of the External Equatorial Shell*

The oscillation amplitudes also depend on the assumed depth of the surface external equatorial shell being modelled, $(r_0' - R_0)/R_1 = H$. In the previous sections, we have maintained $H = 0.01$ which, in essence, assumes that the dominant effect due to the tidal forces is in a layer that extends to a depth of 1% below the stellar surface. An increase in the depth of this layer to $H = 0.03$ in the $R_1 = 18.0\ R_\odot$ model produces an increase in the radial oscillation amplitude, with max(R_{max}) = 18.3 (versus 18.09 for the corresponding model having $H = 0.01$, see Table 2), as well as an increase in the radial velocity amplitude, with $(v_r)_{max} = 7$ km s^{-1} (versus 1.4 km s^{-1} for the corresponding $H = 0.01$ model). From a qualitative standpoint, there is no modification in the behavior of the oscillations with respect to the cases described in the previous sections.

If we fix the value of $H = 0.03$, the radius of the primary star needs to be reduced to $R_1 < 12.6\ R_\odot$ in order for the radial velocity amplitudes to escape detection by the observations. This upper limit to the acceptable stellar radius is lower than that allowed by the observations (Stickland et al. 1987). This leads us to conclude that the value of $H \sim 0.01$ that we have used is justified for the purposes of the present calculations.

4. DISCUSSION AND CONCLUSIONS

We have developed a simple model to calculate the stellar surface deformations and oscillations produced by the tidal interactions in binary systems. We are primarily concerned with exploring in the future the role that these interactions play in producing spectral line profile variability and in possibly modifying the wind structure of massive stars, with respect to the wind structure of analogous single stars. Our model considers only the most external layer of the star, a treatment that is justified 'a posteriori', although it is most likely not valid for the study of the tidal evolution of the system, a problem which at this stage, however, does not concern us. Furthermore, in this preliminary stage, the effects of radiation pressure have not yet been included. Despite these limitations, the model does serve to provide an estimate of the expected magnitude of the bulge amplitude and its orientation, as a function of orbital phase, with respect to the axis of the binary system, as well as the radial velocities associated with the surface displacements. It also provides an estimate of the role played by the kinematical viscosity.

The model is applied to the highly eccentric binary system ι *Ori*, a system that has been used for a variety of studies of the interactions in close binaries, and is currently being used to study the processes of wind-wind interactions. Relevant to the issues of the wind-wind collision, it is important to note that Stevens (1988) modelled the distortion of the primary star at periastron in order to determine the expected change in its mass-loss rate at this phase with respect to other orbital phases. He assumed that the stellar surface lies on an equipotential surface, and thus found that the maximum oscillation amplitude of the bulge is $\sim 2\ R_\odot$ for an $R_1 = 15.8\ R_\odot$ model of the primary, and 0.39 $R_\odot$ for a model with $R_1 = 12.6\ R_\odot$. These values are significantly larger than the values we obtain in this paper ($\sim 0.018\ R_\odot$ and 0.006 $R_\odot$, respectively), indicating that the use of the equipotential surfaces is a poor approximation in non-equilibrium systems such as ι *Ori*. A smaller bulge amplitude implies a smaller difference between the wind structure at periastron and at apastron for this star, according to Stevens' model. Hence, the study of the wind-wind collision at periastron and apastron should at least be free of the complications introduced by variable mass-loss rates.

With respect to the maximum velocity amplitude on the surface of the primary star, we find that under the assumption of $R_1 = 18\ R_\odot$, $(v_r)_{max} \sim 2$ km s^{-1}, for a wide range of values of the kinematical viscosity. This maximum is attained ~ 3 hours prior to the time of periastron passage (Fig. 4*b*). The time-span during which mass motions with velocities larger than 1 km s^{-1} are present is ~ 10 hours. The physical location on the stellar surface where this maximum velocity occurs is at $\Theta = +10°$ with respect to the axis of the binary. Under the assumption that the radius of the primary star is $R_1 = 12.6\ R_\odot$, the maximum velocity amplitudes diminish considerably to $(v_r)_{max} \sim 0.12$ km s^{-1}. For $R_1 = 15.0\ R_\odot$ we obtain $(v_r)_{max} \sim 0.42$ km s^{-1}. The values of $(v_r)_{max}$ for the different assumed values of R_1 and ν are listed in Table 3. Listed also in this table, in the last column, is the azimuth angle, Θ_{vmax}, of the surface element at which $(v_r)_{max}$ occurs.

Gies et al. (1996) observed the system during the orbital phase interval $\Delta\phi = -0.0049 - +0.0030$ around periastron passage. This corresponds to -3.4 to $+2.1$ hours from periastron, a time interval which coincides

TABLE 3

SURFACE RADIAL VELOCITY AMPLITUDES FOR THE PRIMARY STAR IN ι *ORIONIS*

Radius ($R_\odot$)	δ	ν ($R_\odot^2$ day^{-1})	$(v_r)_{max}$ (km s^{-1})	Θ_{vmax} (°)
18.0	0.2	0.07	2.0	+10
18.0	0.2	1.00	1.8	+10
18.0	0.2	10.00	1.8	+10
15.0	0.2	0.1	0.42	+18
12.6	0.2	0.3	0.12	+20

with the maximum velocity amplitudes described in the above paragraph. However, they find no evidence of any systematic profile deviations that can be associated with non-radial pulsations, such as observed in ϵ *Per* (Gies & Kullavanijaya 1988). Gies et al. (1996) estimated a velocity amplitude of 0.65 km s^{-1}, based on a scaling of the model presented by Kumar et al. (1995) and assuming a radius of 15.8 $R_\odot$. Gies et al. (1996) argue that this amplitude should have been within their detection limit. Our value of $(v_r)_{max} = 0.42$ km s^{-1} for the $R_1 = 15$ $R_\odot$ case is slighly smaller, and thus we conclude that the problem presented by the apparent discrepancy between the observations and the predictions of the Kumar et al. (1995) model, is solved by assigning a radius smaller than 15 $R_\odot$ to the primary star. This conclusion supports the results of Stevens (1988), who also favored a smaller radius, on the basis of the terminal velocity of the star and the scaling law between the mass loss rate and stellar radius $\dot{M} \sim R_*^{3.24}$ (Howarth & Prinja 1989).

The model we present also allows an analysis of the role that the kinematical viscosity ν plays in determining the behavior of the stellar oscillations. Very large values of this parameter inhibit large amplitude oscillations; on the other hand, for small values of ν, the solution of the equations of motion for the different surface elements leads them to lose contact between each other and overlap, a phenomenon we associate with turbulence on the model stellar surface. The smallest value of $\nu \sim 0.07$ $R_\odot$ day^{-1} we used in the calculations here corresponds to a dynamical viscosity of $\eta \sim 4 \times 10^{11}$ gm cm^{-1} s^{-1}, for densities in the range of those in giant stars. This viscosity lies near the lower limit of the viscosities demanded by the short timescales for circularization of orbits in massive binaries, as calculated by Alexander (1973) and Sutantyo (1974). Current ideas no longer support this role of turbulent viscosity in producing the circularization of the orbits (Zahn 1975; Goldreich & Nicholson 1989) in early type stars, and given the simplifications in our model, we are unable to contribute to this discussion. However, the fact that small values of ν in our calculations lead to effects that may be associated with turbulence suggests that stars with low surface densities, such as supergiants, may have highly turbulent outer layers when they form part of eccentric binary systems or when they form part of a system which departs significantly from corotation. Thus, some of their atmospheric and wind characteristics could differ from those of comparable single stars. This is an issue of importance which requires further investigation.

We wish to thank an anonymous referee for his comments and suggestions. Support from CONACyT through grant 27744-E is gratefully acknowledged. We thank S. Owocki, A. Maeder, and N. Langer for many helpful discussions.

REFERENCES

Alexander, M. E. 1973, Ap&SS, 23, 459
Corcoran, M. F., et al. 1999, in IAU Symp. 193, Wolf-Rayet Phenomena in Massive Stars and Starburst Galaxies, ed. K. A. van der Hucht, G. Koenigsberger, & P. R. J. Eenens (Dordrecht: Reidel), 772
Fehlberg, E. 1968, NASA, TR R-287
Gies, D. R., Barry, K. J., Bagnuolo, W. G., Sowers, J., & Thaller, M. L. 1996, ApJ, 469, 884
Gies, D. R., & Kullavanijaya, A. 1988, ApJ, 326, 813
Giuricin, G., Mardirossian, F., & Mezzetti, M. 1984a, A&A, 131, 152
_____. 1984b, A&A, 134, 365
_____. 1984c, A&A, 135, 393
Goldreich, P., & Nicholson, P. D. 1989, ApJ, 342, 1079
Howarth, I. D., & Prinja, R. K. 1989, ApJS., 69, 527
Hut, P. 1980, A&A, 92, 167

_____. 1981, A&A, 99, 126
Koenigsberger, G., & Moreno, E. 1997, in ASP Conf. Ser. Vol. 120, Luminous Blue Variables: Massive Stars in Transition, ed. A. Nota & H. Lamers (San Francisco: ASP), 332
Koenigsberger, G., Moreno, E., Cantó, J., & Raga, A. 1999, in IAU Symp. 193, Wolf-Rayet Phenomena in Massive Stars and Starburst Galaxies, ed. K. A. van der Hucht, G. Koenigsberger, & P. R. J. Eenens (Dordrecht: Reidel), 38
Kumar, P., Ao, C. O., & Quataert, E. J. 1995, ApJ, 449, 294
Landau, L. D., & Lifshitz, E. M. 1984, Fluid Mechanics, (Oxford: Pergamon Press)
Lang, K. R. 1986, Astrophysical Formulae, Springer-Verlag, ISN 0-387-09933-6 (NY-Heidelberg-Berlin: Springer-Verlag), 546
Marchenko, S. V., et al. 2000, in preparation
Pittard, J. 1998, MNRAS, 300, 479
Pittard, J., Stevens, I. R., Corcoran, M. F., Gayley, K. G., Marchenko, S. V., Rauw, G., & Torii, K. 2000, MNRAS, submitted
Press, W. H., & Teukolsky, S. A. 1977, ApJ, 213, 183
Press, W. H., Wiita, P. J., & Smarr, L. L. 1975, ApJ, 202, L135
Savonije, G. J., Papaloizou, J. C. B., & Alberts, F. 1995, MNRAS, 277, 471
Stevens, I. R. 1988, MNRAS, 235, 523
Stickland, D. J., Pike, C. D., Lloyd, C., & Howarth, I. D. 1987, A&A, 184, 185
Sutantyo, W. 1974, A&A, 35, 251
Symon, K. R. 1971, Mechanics (Reading, MA: Addison-Wesley)
Verbunt, F., & Phinney, E. S. 1995, A&A, 296, 709
Zahn, J.-P. 1975, A&A, 41, 329
_____. 1977, A&A, 57, 383
_____. 1989, A&A, 220, 112

Gloria Koenigsberger and Edmundo Moreno: Instituto de Astronomía, UNAM, Apartado Postal 70-264, 04510 México, D.F., México (edmundo, gloria@astroscu.unam.mx).